Fe (PB)-P-Se NANOCUBES AS HER ELECTROCATALYSTS FOR OVERALL EFFICIENT WATER-SPLITTING

M. AHMED[a, b,*], M. N. LAKHAN[a,b], Y. TIAN[a,b], A. H. SHAR[a,b], J. YU[a,b],
I. ALI[c], J. LIU[a,b], J. WANG[a,b]
[a]*Key Laboratory of Superlight Material and Surface Technology, Ministry of Education, Harbin Engineering University, PR People's Republic of China.*
[b]*College of Material Science and Chemical Engineering, Harbin Engineering University, PR People's Republic of China*
[c]*College of Chemical Engineering, Beijing University of Chemical Technology, PR People's Republic of China*

In recent times, selecting an effective electrocatalyst has attracted a lot of attention for improving the efficiency of water splitting to obtain clean fuels as an energy carrier. In this study, a self-pattern strategy is reported to synthesize Selenide (Se)-Phosphate (P) mixed Prussian blue (PB) cubic nanocubes for the electrocatalytic hydrogen evolution reaction (HER). The as-prepared nanocubes were characterized by different techniques. SEM and TEM confirm that the nanocube structure has been successfully formed. XRD pattern obtained peaks meets with the standard JCPDS no. 01-0239.The resulting P-Se mixed nanocubes worked as a superior HER electrocatalyst, which affords a current density of 10 mA cm^{-2}at a small overpotential of 210mV; at the overpotential of 211mV; a Tafel slope as 147 mV/dec in 1M KOH; and excellent stability in alkaline medium. From results, we affirmed that Prussian based nanocubes can work with great potential in water splitting.

1. Introduction

Recently, the key challenge is to discover renewable clean energy as an alternative source for fossil fuels and to find efficient energy storage devices [1, 2]. Electrochemical water-splitting is one of the ideal methods to generate hydrogen fuel as a clean energy resource with its high energy storage density and very less carbon emission. Splitting of water into hydrogen and oxygen ($2H_2O \rightarrow 2H_2 + O_2$) provides a new procedure to produce renewable energy sources [1]. Hydrogen is considered as one of the most promising energy carriers due to its clean and renewable nature [3]. Among the various hydrogen generation techniques, water splitting attracts great attention due to its sustainability and eco-friendly properties [4, 5]. Catalysts play a vital role in the hydrogen evolution reaction (HER) to generate hydrogen efficiently from water [6, 7]. During this reaction, hydrogen production is an endothermic reaction which often requires expensive catalysts like platinum to attain a satisfactory rate of production. Unfortunately, currently, present Pt-group metals exhibit the excellent HER catalytic performance is rare and expensive, which limits their applicability [8]. Therefore, developing earth-generous alternative catalysts with high HER activity is a big challenge for scientists due to the cost-effective production of hydrogen [9, 10]. Recent research on hydrogen provides a new era to design advanced HER catalysts [11, 12]. Several kinds of reasonable transition metal sulfides and phosphates have been investigated as efficient HER electrocatalysts [12-15]. During the water-splitting reaction hydrogen and oxygen are produced simultaneously [16]. Several investigations have been carried out to generate cost-effective catalysts for water splitting which elaborate properties of electrocatalysts such as electrochemically active surface area, resistance to charge transfer, morphology, specific activity, and stability [17, 18]. Prussian blue has unique properties such as electrochemical, photophysical,

---

* Corresponding author: ahmedmukhtiar461@gmail.com

magnetic, and has a perfect catalytic activity to gain hydrogen peroxide [19-23]. Prussian blue (PB) based materials are being studied extensively owing to their inexpensiveness and highly efficient HER electrocatalysts performance [24-26]. Moreover, the behavior of sodium bi-hydrogen phosphate (NaH_2PO_4) and selenium (Se) in Prussian blue (PB) is favorable and has good capability solutions to the introductory problems due to its excellent properties [27]. PB-based nanocube structure materials are typically prepared via proper mixing method [28]. Moreover, Prussian blue-selenide-phosphates with crystalline character can be imposed with greater interest considering their good electronic conductivity and fast electron-transport ability over those recently reported materials for electrochemical applications [29, 30]. Herein, we first developed Fe (PB)-P-Se nanocubes and then treated it on a Ni foam surface Fe (PB)-P-Se/NF via an *in situ* electrodeposition method. By treating material at different range of electrodeposition times, results show that Fe (PB)-P-Se exhibits the best HER catalytic activity in 1 M KOH in alkaline medium, which only requires an overpotential of 210 mV to initiate the reaction and can provide current densities of 10 and 100 mA cm^{-2} at over potential as of 211 and 270, respectively. Furthermore, cubic Fe (PB)-P-Se showed excellent electrocatalytic stability within the required time [31, 32].
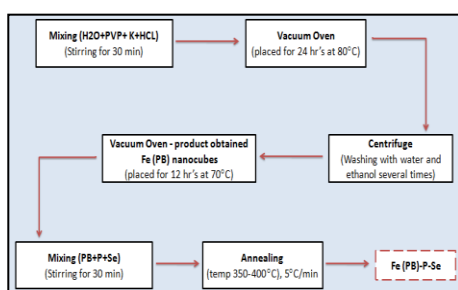
Fig. 1. Schematic process flow diagram of Fe (PB)-P-Se preparation.

2. Material and methods

2.1. Materials and reagents

Polyvinylpyrrolidone (C_6H_9NO) and pure selenium powder (Se) were purchased from Sinopharm chemical reagents Co. LTD, Potassium ferrocynide $K_4\{Fe(CN)_6\}$, dilute hydrochloric acid (HCL), Sodium dihydrogen phosphate (NaH_2PO_4) obtained from Tianjin Yaohua chemical reagents Co. LTD. 1cm×1cm piece of nickel foam was used. All types of equipment were gently washed and deionized water was used in experiments.

2.2. Preparation of Fe (PB)-P-Se

In a typical synthetic procedure for the Synthesis of Fe(PB)-P-Se nanocubes, 10.0g of PVP (C_6H_9NO) n, 0.55g of Potassium ferrocynide $K_4\{Fe(CN)_6\}$, 1.67g of Hydrogen chloride (HCL) were dissolved in 200 ml of distilled water under stirring for 30 min. then, the PB obtained mixed solution was heated at a temperature of 80°C for 24h in a vacuum oven. Later, the obtained PB product was centrifuged and washed several times with distilled water and ethanol for 10 minutes. The centrifuged PB product was collected and dried in a vacuum oven for overnight at 70°C. Then the PB was mixed with elements such as P, Se, and P-Se to prepare three different composites (PB-P, PB-Se, and PB-P-Se) by annealing. Subsequently, 0.25g of NaH_2PO_4 and 0.2g of Selenium (Se) were positioned in the upstream and 0.42g of PB as-obtained was placed downstream in the tube furnace so that PB-Se-P can be sufficiently contacted with the gas stream. Under a nitrogen atmosphere, the furnace was heated to 400°C for 3 hours with a heating rate of 5°C/min^{-1}. On cooling down the temperature to room temperature, the product denoted as PB-Se-P Se was obtained. The electrodeposition was carried out in a standard three-electrode electrochemical cell with Ni foam as the working electrode, an Hg/Hg^o as the reference electrode and a parallel positioned platinum wire as the auxiliary electrode. The electrolyte bath contained 0.45 ml DI

water, 0.45 ml ethanol, 0.1 ml of Nafion and 0.05g of a sample. The electrodeposition was then carried out with cyclic voltammetry by sweeping the potential from 0 to 1 V vs. Hg/Hg^o with the scan rate of 100 mV s^{-1}.

2.3. Structural characterization

The morphology and structure of the microspheres were characterized by Scanning Electron Microscopy (SEM, JSM-6480A, JOEL) run at 20 kV an accelerating voltage, elemental mapping, Energy-disperse X-ray (EDX) spectroscopy were obtained using JSM-6480A, JOEL, Transmission Electron Microscopy (TEM, Tecnai-G220S-Twin, FEITEM) at 120 kV an accelerating voltage. The X-ray diffraction (XRD) patterns were taken in an X-Ray Diffraction (XRD, Rigaku TTR-III) operated at 40 kV/150 mA with high-intensity Cu Ka radiation (λ=0.15406 nm) and X-ray photoelectron spectroscopy (XPS) measurements were performed using a PHI 5700 ESCA spectrometer with Al KR radiation (hv= 1486.6 eV).

2.4. Electrocatalytic measurements

All electrochemical measurements were carried out in 1 M KOH solution using a CHI760E electrochemical workstation (Shanghai Chenhua Instrument Co. Ltd.) with a standard three-electrode system. The prepared PB-P-Se electrode was used as the working electrode, Hg/Hg^o as the reference electrode and the platinum (Pt) as the auxiliary electrode. During the experiment, the iR dropped from the solution was corrected. All electrochemical measurements were carried out at room temperature. The polarization curves were recorded with a scan rate of 2 mV s^{-1} by sweeping the potential from 0 to 1 V vs Hg/Hg^o. The working electrode is activated several times to stabilize the signal. The Tafel slope is obtained from the polarization curve. Electrochemical surface area (ECSA) was obtained by measuring the capacitive current which was associated with double-layer charging from the scan-rate dependence of CVs. The potential was in the range of 0-0.1 V (vs. Hg/Hg^o). The scan rates were 20, 40, 60, 80, 100, 120, 140, 160, 180 and 200 mV s^{-1}, respectively. The double-layer capacitance (Cdl) was obtained from the plot of charging current difference –j at 0.05V (vs. Hg/Hg^o) with the scan rate. The slope is twice of the double-layer capacitance Cdl. Electrochemical impedance spectroscopy (EIS) was carried out in 1.0 M KOH aqueous solution by applying an alternating current (AC) voltage of 5 mV amplitude in a frequency range from 100 kHz to 0.1 Hz at a potential of 0.52 V (vs. Hg/Hg^o).

3. Results and discussion

Fe(PB)-P-Se is synthesized by a one-step method, an annealing process followed by a phosphidation and selenation process by flowing nitrogen gas into the annealing tube as shown in Fig. 1. The structure and phase purity of Fe(PB)-P-Se was monitored by X-ray diffraction (XRD) as depicted in Fig. 2. XRD pattern shows different diffraction peaks centered at 17.23°, 24.65°, and 35.18° can be well indexed to the substrate, and other peaks centered at 33.5°, 39.4°, 43.6°, 50.6°, 53.9°, 57.1° and 70.0° [33]. Among them, sharp diffraction peaks are consistent with the standard Fe-P-Se (JCPDS no. 01-0239), and some diffraction peaks formed due to the impurities observed in a pattern. XRD pattern indicates that good crystallinity nanocubes structure formed.
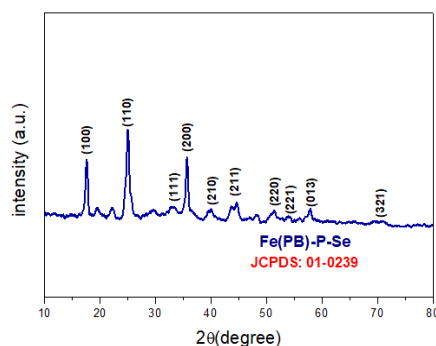
Fig. 2. XRD pattern of Fe (PB)-P-Se *powders annealed by annealing tube, at temperature 350–400°C.*

The morphology of the annealed product was observed by Scanning electron microscopy (SEM) images as shown in Fig. 3(a-d). Fig. 3(a) shows that the pure Prussian blue structure was uniform and of cubic shape. Fig. 3(b) presents the cubic structure of Fe (PB)-P. Fig. 3(c) shows the Fe(PB)-Se nanocube structure [34]. As in Fig. 3(a) each Fe(PB) cube contain eight angles (corners) all are uniformed, after treatment with Selenium(Se) and phosphate(P) individually and also together for 3h in annealing tube, Fig. (b, c, and d) shows that Fe(PB)-P, Fe(PB)-Se and Fe (PB)-P-Se could remain the cube morphology [35], relatively better than pure Fe(PB) which suffered from serious bulk between the particles. The Fe (PB)-P-Se samples are nanocubes with high crystallinity at high or low magnification, it was obvious to find that most crystals were intact and having regular morphology for better and efficient water [36].
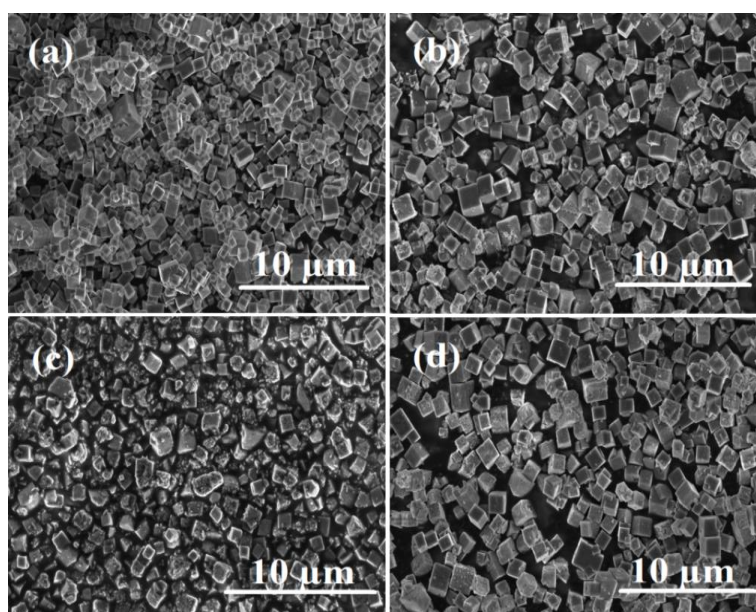
Fig. 3 SEM images of (a) Fe(PB), (b)Fe(PB)-P, (c)Fe(PB)-Se and (d) Fe (PB)-P-Se.

The morphology of the product was examined by Transmission electron microscopy (TEM) images as shown in Fig. 4(a-f). The nanocubes are not balanced but uniformly distributed from 1μmto 10nm, a certain change in the nanocubes is due to the as-obtained Fe(PB) were subjected to chemical treatment with Selenium (Se) and phosphate (P). However, the treatment of Fe(PB) with Se and P in annealing tube leads to the ordering of the nanocube structures by decreasing the bulk between cubes. Therefore, Fe(PB)-P-Se becomes more arranged when

compared with Fe(B) [37, 38]. In the figure, you can see that that iron (Fe), Phosphate (P) and Selenium (Se) are uniformly distributed in these nanocubes.
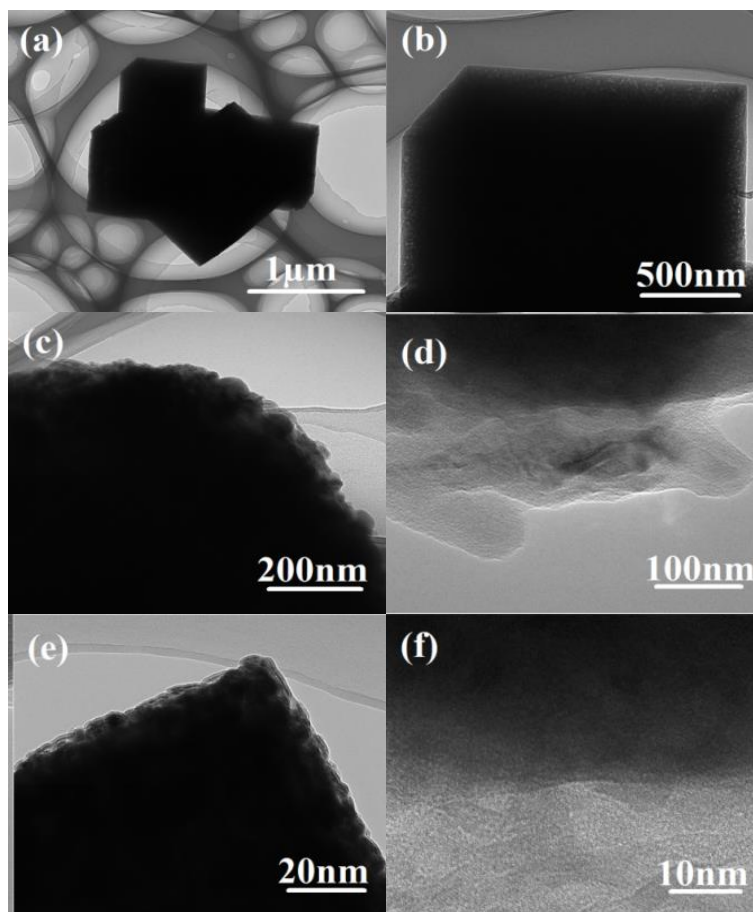
Fig. 4. Low to the high-resolution TEM image of as-prepared Fe(PB)-P-Se.

The Energy-dispersive X-ray spectroscopy (EDS) spectrum reveals that the Fe(PB)-P-Se contains elemental Fe, P, and Se. EDS elemental analysis further confirms that Fe(PB)-P-Se nanocubes are composed of Fe, P, Se, K, C, and N [39] elements and that these elements are uniformly distributed from the EDS element mappings.
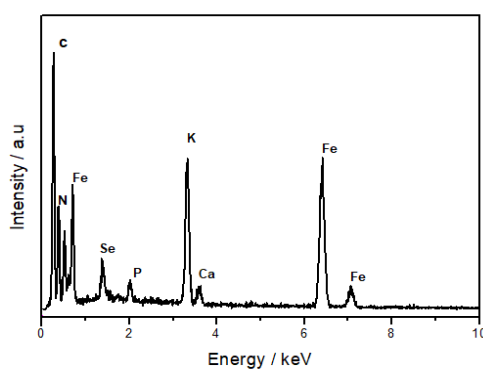
Fig. 5 EDS spectrum of Fe(PB)-P-Se

The electrocatalytic performance of the Fe(PB)-P-Se electrode for the HER was investigated in an alkaline medium as depicted in Fig. 6. The HER performance of Fe(PB)-P-Se was evaluated by linear sweep voltammetry (LSV) in 1 M KOH solution. For comparison, samples prepared by electrodeposition for Fe(PB), Fe(PB)-P, Fe(PB)-Se and Fe(PB)-P-Se were also studied. Showing that the Fe(PB)-P-Se exhibits a decrease in reaction energy for water reduction into hydrogen. In addition, the sample also exhibits good catalytic activity towards the HER with overpotentials of Fe(PB)-P-Se 103 mV at current density of 10 mA cm^{-2} and 330 mV at 100 mA cm^{-2}, lower than Fe(PB),Fe(PB)-P and Fe(PB)-Se which showed overpotentials of 379, 205 and 356mV at 100 mA cm^{-2}respectively [39].
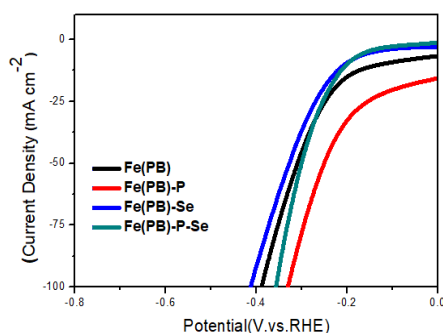
Fig. 6. LSV polarization curves for HER in the KOH medium.

The Tafel plots were derived from the linear sweep voltammetry (LSV) polarization curves using the Tafel equation $\eta = b \log (j) + a$, where η is the overpotential, j is the current density, and b is the Tafel slope. The Fe(PB)-P-Se nanocubes possess the Tafel slope of 147 mV dec^{-1}, indicate the most favorable reaction kinetics for HER as presented in Fig. 7. Fe(PB), Fe(PB)-P, and Fe(PB)-Se NCs also show Tafel slope of 224 mV dec^{-1}, 314 mV dec^{-1} and 175 mV dec^{-1}. However, on Fe(PB)-P-Se nanocubes, HER follows the Volmer−Heyrovsky mechanism, where Volmer step is the rate-determining step [40].
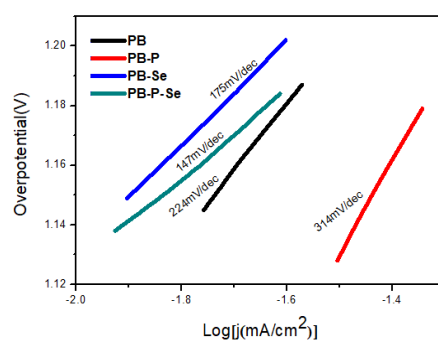
Fig. 7 Tafel slopes of Fe(PB), Fe(PB)-P, Fe(PB)-Se and Fe(PB)-P-Se.

The Cyclic voltammograms (CVs) were collected in the region of 0.27–0.37 V. The CVs recorded at various scan rates are displayed in Fig. 8 for the better interpretation and comparison [39], Cyclic voltammograms (CV) of Fe(PB)-P-Se measured in 1 M KOH solution in a potential window without faradaic processes (scan rate: 20, 40, 60, 80, 100, 120, 140, 160, 180 and 200 mV/s) [41].
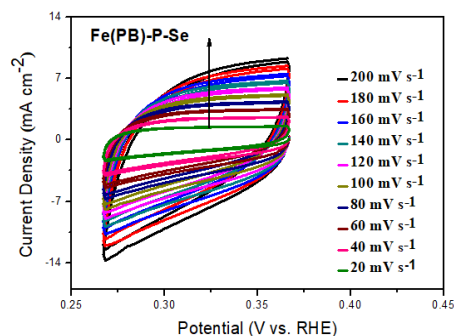
Fig. 8. Cyclic voltammetry curves of Fe(PB)-P-Se /NF electrode at different scan rates.

The capacitance for Fe(PB)-P-Se is 3.44 mF cm-2 as shown in Fig. 9. Therefore, high performance could be associated with the high electro-active surface area [42]. The measured active surface area is not an absolute value; however, it could serve as a guide for the comparison of surface roughness for similar materials.
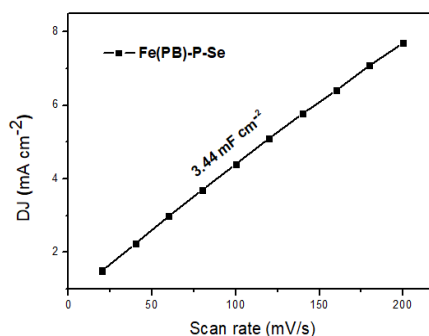
Fig. 9. The double-layer capacitance scan rate.

Electrical impedance spectroscopy (EIS) at various overpotentials was employed to further gain more insight into the interface reaction and electrode kinetics of Fe(PB)-P-Se towards HER as presented in Fig. 10 [43]. The electrochemical impedance spectroscopy (EIS)was then measured -141 mV and the R_{ct} of Fe(PB)-P-Se (50 Ω) Therefore, the high effective surface area and low charge resistance suggest that Fe(PB)-P-Se composite can provide more active sites and facilitate fast charge transfer during the HER process in 1M KOH solution, leading to its superior catalytic performance.
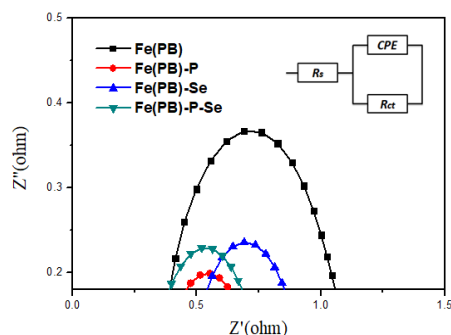
Fig. 10. EIS of the Fe(PB), Fe(Pb)-P, Fe(PB)-Se and Fe(PB) in 1 M KOH solution
with an over the potential of 250 mV.

4. Conclusion

In this article, we have explored a series of methods to design nanostructure catalysts for water splitting, including hydrothermal method, Annealing method; chemical redox reaction; hard template method and electron deposition technique successfully for the preparation of Prussian blue (PB) based materials as the catalysts towards HER. The as-prepared Fe(PB)-P-Se results in the reduction in the HER energy barrier and to accelerate the overall water splitting process. Therefore, Fe(PB)-P-Se showed excellent HER performance with overpotentials of 211 and 270 mV to reach 10 and 100 mA cm^{-2} in alkaline media (1M KOH). It was affirmed that these nano-structured catalysts simultaneously generate H_2 in alkaline solution and exhibit excellent catalytic activity and stability towards water splitting.

References

[1] S. N. Lewis, D. G. Nocera, Proceedings of the National Academy of Sciences of the United States of America **103**(43), 15729 (2006).

[2] B. M, Hunter, H. B. Gray, A. M. Muller, Chemical Reviews **116**(22), 14120 (2016).

[3] S. N. Lewis, D. G. Nocera, Proceedings of the National Academy of Sciences oth the United States of America **103**(43), 15729 (2006).

[4] J. A. Turner, Science **305**(5686), 972 (2004).

[5] I. Roger, M. A. Shipman, M. D. Symes, Nature Reviews Chemistry **1**(1), (2017).

[6] A. B. Laursen, S. Kegnæs, S. Dahl, Ib. Chorkendorff, Energy & Environmental Science **5**(2), 5577 (2012)

[7] C. G. Morales-Guio, L. A. Stern, X. Hu, Chemical Society Reviews **43**(18), 6555 (2014).

[8] Y. Jiao, Y. Zheng, M. Jaroniec, S. Z. Qiao, Chemical Society Reviews **44**(8), 2060 (2015).

[9] U. K. Sultana, A. P. O'Mullane, ACS Applied Energy Materials **1**(6), 2849 (2018).

[10] M. S, Faber, S. Jin, Energy Environmental & Energy **7**(11), 3519 (2014).

[11] Y. Shi, B. Zhang, Chemical Society Reviews **45**(6), 1529 (2016).

[12] H. I. Karunadasa, E. Montalvo, Y. Sun, M. Majda, J. R. Long, C. J. Chang, Science **335**(6069), 698 (2012).

[13] B. Hinnemann, P. G. Moses, J. Bonde, K. P. Jørgensen, J. H. Nielsenand, S. Horch, Ib. Chorkendorff, J. K. Nørskov, JACS Communication **75**(127), 610 (2015).

[14] B. Hinnemann, P. G. Moses, J. Bonde, K. P. Jørgensen, J. H. Nielsen, S. Horch, Ib. Chorkendorff, J. K. Nørskov, Journal of American Chemical Society **27**, 5308 (2005).

[15] M. S. Faber, R. Dziedzic, M. A. Lukowski, N. S. Kaiseret, Q. Ding, S. Jin, Journal of the American Chemical Society **136**(28), 10053 (2014).

[16] Y. Li, H. Wang, L. Xie, Y. Liang, G. Hong, H. Dai, Journal of the American Chemical Society **133**(19), 7296 (2011).

[17] D. Voiry, H. Yamaguchi, J. Li, R. Silva, D. C. B. Alves, T. Fujita, M. Chen, T. Asefa, V. B. Shenoy, G. Eda, M. Chhowalla, Nature Materials **12**(9), 850 (2013).

[18] S. Anantharaj, S. R. Ede, K. Sakthikumar, K. Karthick, S. Mishra, S. Kundu, ACS Catalysis **6**(12), 8069 (2016).

[19] Y. Qu, Mi. Yang, J. Chaiet, Z. Tang, M. Shao, C. T. Kwok, M. Yang, Z. Wang, D. Chua, S. Wang, Z. Lu, H. Pan, ACS Applied Materials & Interfaces **9**(7), 5959 (2017).

[20] Y. Ji, L. Yang, X. Ren, G. Cui, X. Xiong, X-P. Sun, ACS Sustainable Chemistry & Engineering **6**(8), 9555 (2018).

[21] A. M. Farah, C. Billing, C. W. Dikio, A. N. Dibofori-Orji, O. O. Oyedeji, D. Wankasi, F. M. Mtunzi, E. D. Dikio,International Journal of Electrochemical Science **8**, 12132 (2013).

[22] L. Cui, J. Zhu, X. Meng, H. Yin, Xi. Pan, S. Ai, Sensors and Actuators B: Chemical **161**(1), 641 (2012).

[23] A. M. Farah, N. D. Shooto, F. T. Thema, J. S. Modise, E. D. Dikio, International Journal of Electrochemica lScience **7**, 4302 (2012).

[24] J. Zeng, W. Wei, X. Liu, Y. Wang, G. Luo, Microchimica Acta **160**(1-2), 261 (2007).

[25] J.-Z. Tao, G.-R. Xu, H.-L. Hao, F.-X. Yang, K.-S. Ahn, W.-Y. Lee, Journal of Electroanalytical Chemistry **689**, 96 (2013).

[26] S. Du, Z. Ren, Y. Qu, J. Wu, W. Xi, J. Zhu, H. Fu, Chemical Communications **52**, 6705 (2016).

[27] H. Zhu, J. Zhang, R. Yanzhang, M. Du, Q. Wang, G. Gao, J. Wu, G. Wu, M. Zhang, B. Liu, J. Yao, X. Zhang, Advanced Materials **27**(32), 4752 (2015).

[28] L. Cao, F. Xu,Y.-Y. Liang, H.-L. Li, Advanced Materials **16**(20), 1853 (2004).

[29] X. Teng, J. Wang, L. Ji, W. Tang, Z. Chen, ACS Sustainable Chemistry & Engineering **6**(2), 2069 (2017).

[30] J. Nai,X.W. D. Lou, Advanced Materials **31**(38), 1706825 (2019).

[31] Y. Liu, J. Goebl, Y. Yin, Chemical Society Reviews **42**(7), 2610 (2013).

[32] A. Indra, U. Paik, T. Song, Angewandte Chemie **57**(5), 1241 (2018).

[33] X. Lu, C. Zhao, Nature Communications **6**, 6616 (2015).

[34] H. Liang, F. Meng, M. Cabán-Acevedo, L. Li, A. Forticaux, L. Xiu, Z. Wang, S. Jin, Nano Letters **15**(2), 1421 (2015).

[35] C. Wang, J. Jiang, T. Ding, G. Chen, W. Xu, Q. Yang, Advanced Materials Interfaces **3**(4), 1500454 (2016).

[36] C. Xuan, J. Wang, W. Xia, Z. Peng, Z. Wu, W. Lei, K. Xia, H. L. Xin, D. Wang, ACS Applied Materials & Interfaces **9**(31), 26134 (2017).

[37] L. Han, X.Y. Yu, X. W. Lou, Advanced Materials **28**(23), 4601 (2016).

[38] L. Zhang,H. B. Wu, X. W. Lou, Journal of American Chemical Society **135**(29), 10664 (2013).

[39] L. Zhang, T. Meng, B. Mao, D. Guo, J. Qin, M. Cao, RSC Advances **7**(80), 50812 (2017).

[40] L-P. Wang, P-F. Wang, T-S. Wang, Y-X. Yin, Y-G. Guo, C-R. Wang, Journal of Power Sources **355**, 18 (2017).

[41] P. Jiang, Q. Liu, Y. Liang, J. Tian, A. M. Asiri, X. Sun, Angewandte Chemie **53**(47), 12855 (2014).

[42] B. Yuan, F. Sun, C. Li, W. Huang, Y. Lin, Electrochimica Acta **313**, 91 (2019).

[43] D. Kong, H. Wang, Z. Lu, Y. Cui, Journal of American Chemical Society **136**(13), 4897 (2014).